The Seismic Record
A journal of the Seismological Society of America

Source Separation and Medium Change of Contained Chemical Explosions from Coda Wave Interferometry

Sean R. Ford*[1] and William R. Walter[1]

Abstract

Differences in the seismic coda of neighboring events can be used to investigate source location offsets and medium change with coda wave interferometry (CWI). We employ CWI to infer the known relative location between two chemical explosions in Phase I of the Source Physics Experiment (SPE). The inferred displacement between the first, SPE-1, and second, SPE-2, chemical explosion is between 6 and 18 m, with an expectation of 9.2 m, where the known separation is close to 9.4 m. We also employ CWI to find any velocity perturbation due to damage from SPE-2, by comparing its coda with the collocated third SPE chemical explosion, SPE-3. We find that damage due to SPE-2 must be confined to a spherical region with radius less than 10 m and velocity perturbation less than 25%.

Cite this article as Ford, S. R, and Walter, W. R (2021). Source Separation and Medium Change of Contained Chemical Explosions from Coda Wave Interferometry, *The Seismic Record*. **1**, 3–10, doi: 10.1785/0320210002.

Introduction

The Source Physics Experiment (SPE) is a multiphase experiment to better understand explosion physics and, thereby, improve explosion monitoring (Snelson *et al.*, 2013). The first part, Phase I, examined the explosion source in a hard-rock medium and took place in a granite outcrop of the Climax Stock section (Townsend *et al.*, 2011) of the Nevada National Security Site (Fig. 1, inset). Events from this series of chemical explosions in saturated granite are usually referred to simply as the SPE events (i.e., SPE-1, SPE-2, etc.).

All shots were recorded on a local network of short-period seismometers (Fig. 1), and we employ these recordings in the analysis. Figure 2 shows recordings of the SPE Phase I chemical explosions from this network. The great difference in the waveforms is primarily due to differences in path heterogeneity, which is difficult to model. However, differential measurements of sources recorded at the same site do not suffer from these complications and can get at near-source properties more directly (Poupinet *et al.*, 1996). Poupinet *et al.* (2008) gives a good review of differential measurement techniques. One of the methods—coda wave interferometry (CWI)—has shown promise in finding very small changes in source and medium properties. Snieder and Hagerty (2004) measured changes in volcanic tremor location, and Grêt *et al.* (2006) measured medium velocity perturbation due to an imposed stress change using CWI. We will use CWI to infer small changes in the near-source environment of the SPE explosions due to damage and test the ability to retrieve known source location offsets.

It is important to quantify the damage component of the seismic wavefield to better understand the effects of source, path, and site. Johnson and Sammis (2001) found that the damage radius is up to 10 times the post-shot cavity radius and is a separate source of seismic radiation that must be accounted for. Patton and Taylor (2011) attempt to quantify the contribution of late-time damage to seismic moment and find that it is significant for certain emplacement conditions. Modeling of the 1993 "tuna-can" shaped Non-Proliferation Experiment explosion by Stevens and O'Brien (2012) shows a somewhat spherical damage region, and Martin *et al.* (2011) report a velocity change of 20% in the near-source region due to damage in granite for an experiment in Vermont that could affect shear-wave generation

1. Lawrence Livermore National Laboratory, Livermore, California, U.S.A., https://orcid.org/0000-0002-0376-5792 (SRF); https://orcid.org/0000-0002-0331-0616 (WRW)

*Corresponding author: sean@llnl.gov

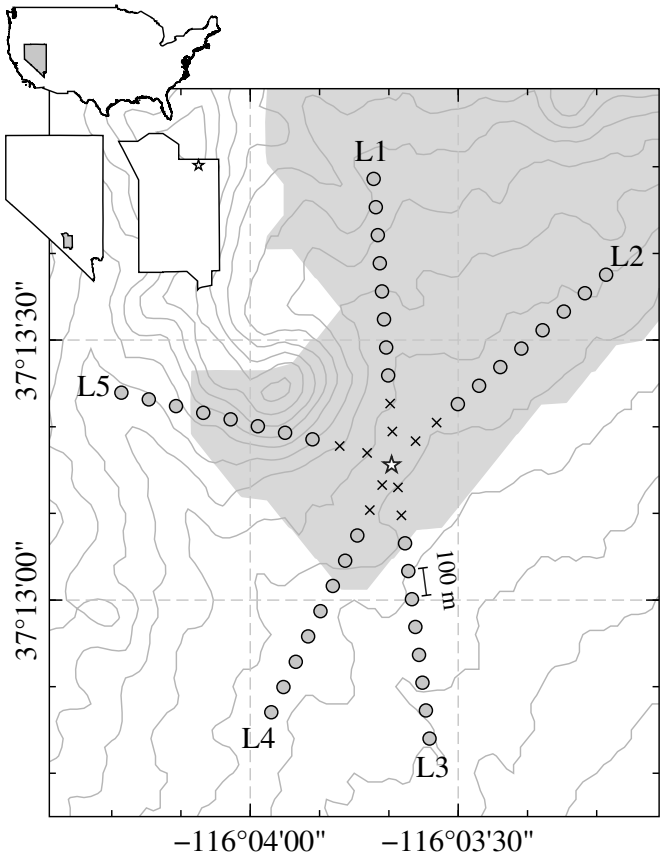

Figure 1. Source–station geometry of the Source Physics Experiment (SPE), Phase I. Stations have 100 m spacing, where the lines are listed at the end (e.g., L1), and the station numbers increase from 1 to 10 as distance from source (star) increases. Stations used in the analysis are marked with circles (unused stations marked with ×). Elevation contours are at 20 m intervals, and the Climax Stock granite outcrop is shown in gray. The inset maps give the location of the SPE.

(Stroujkova *et al.*, 2012). The use of CWI with the well-studied SPE explosions offers a unique opportunity to assess its use in other experiments and at other nuclear test sites. This observational study will focus on applying the CWI method to SPE data, and future work will focus on detailed numerical and physical modeling of how such damage can occur.

Data

The first chemical explosion, SPE-1, intended as a calibration shot, consisted of 87.9 kg trinitrotoluene (TNT)-equivalent (1 kg TNT-equivalent is 4184 kJ) of sensitized heavy ammonium nitrate fuel oil (SHANFO) loaded into a right circular cylinder canister with a diameter and height of, approximately, 0.5 m and lowered to a source centroid depth of 55.1 m. The next two shots, SPE-2 and SPE-3, were approximately the same size, and consisted of 997 and 905 kg TNT-equivalent of SHANFO, respectively, loaded into right circular cylinder canisters with a diameter of 0.8 m, and height of 3 and 2.7 m, respectively, and lowered to source centroid depths of 45.7 and 45.8 m, respectively. These shots were intended to examine effects of rock damage on explosion signals.

A variety of instruments were deployed in five lines extending radially away from the shot point. In this study, we focus on the closest surface instruments, which are short-period (4.5 Hz corner) GS11D vertical-component geophones. The geophones were deployed at 100 m intervals and installed on concrete pads set into the surface. Geophones at a distance less than 200 m from SPE-2 and SPE-3 exceeded the sensor measurement range (i.e., "clipped"), so we do not include them in the analysis (indicated by × in Fig. 1). In addition, recordings of SPE-1 at L4-06, SPE-2 at L2-09, L4-07, and L5-03, and SPE-3 at L2-01, L2-03, L3-03, L4-07, L5-09, and L5-10 had problems (e.g., dropouts, sensor noise, and altered sensor locations) and are not employed in the analysis. These traces are zeroed out in Figure 2.

Coda Wave Interferometry (CWI)

CWI is a powerful technique for detecting small changes in source and structure parameters from repeated explosions (Snieder *et al.*, 2002). The improved detection capability is due to exploitation of the Earth as a multiply scattering medium so that it can be used as an interferometer. Small changes in the scattering medium can be detected as small time shifts in the coda of seismic waves that sample the medium. The theory presented here follows Robinson *et al.* (2007).

The normalized time-shifted cross correlation is given by

$$R^{(t,t_w)}(t_s) = \frac{\int_{t-t_w}^{t+t_w} u(t')\hat{u}(t'+t_s)dt'}{\sqrt{\int_{t-t_w}^{t+t_w} u^2(t')dt' \int_{t-t_w}^{t+t_w} \hat{u}^2(t')dt'}}, \quad (1)$$

in which t_s is the shift time, and $R^{(t,t_w)}(t_s)$ measures the change between the reference u and perturbed $\hat{u}$ scattered velocity field over a time window of length $2t_w$. The cross correlation attains its maximum value $R_{\max}^{(t,t_w)}$ when $t_s = \langle\tau\rangle_{(t,t_w)}$, which is the mean travel-time perturbation of the arrivals in the time window. Snieder (2004) shows that an appropriately large t_w of about five times the dominant period of the waveform is needed to stabilize the measurement. Each of these windows of $2t_w$ length offers an independent assessment of t_s, so a stable observation can be found from repeated measurement windows. In addition, noise can contaminate the late-time coda wave

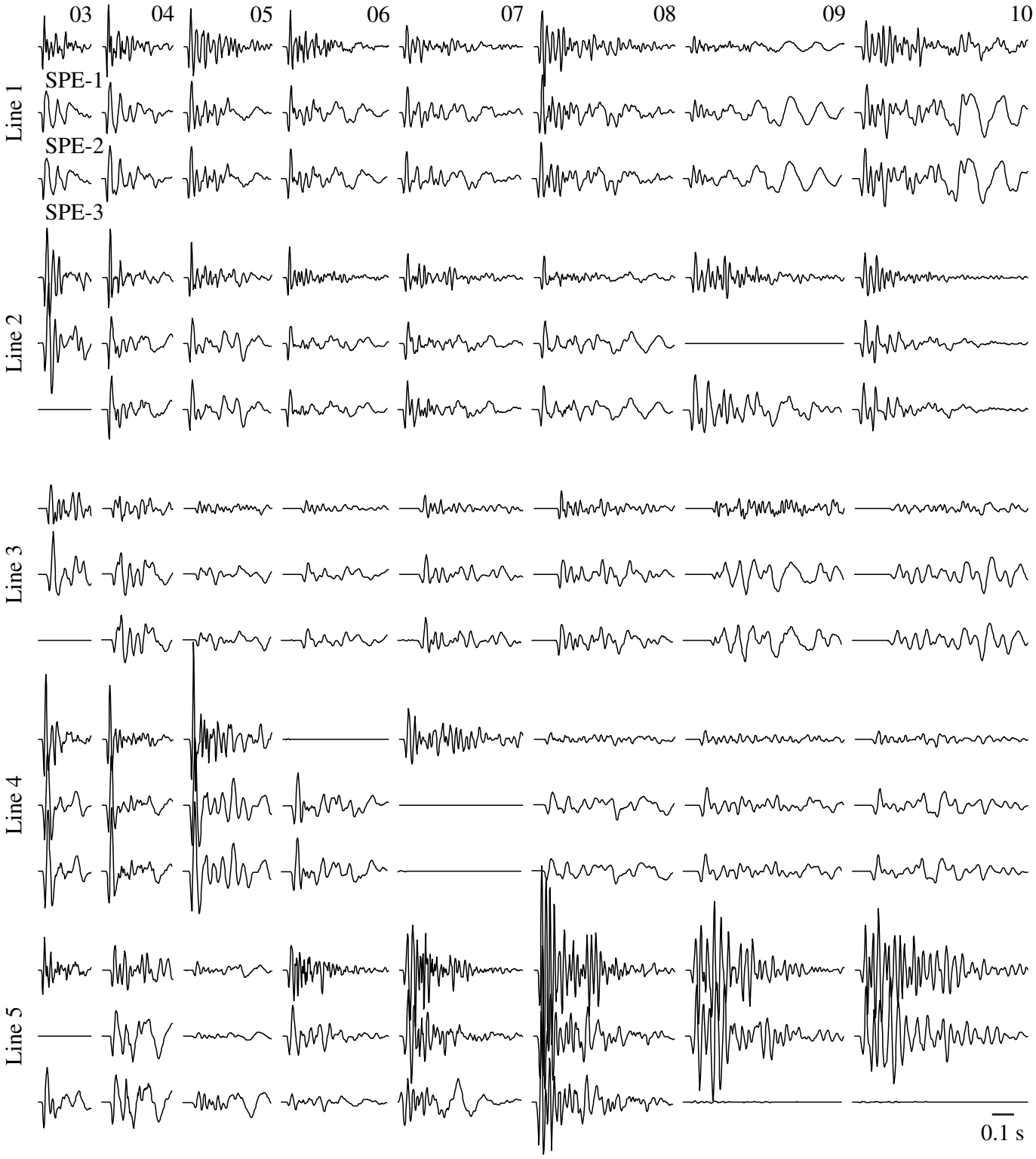

Figure 2. Vertical geophone recordings of the SPE explosions. Traces are scaled by distance, where the station number is also the approximate distance divided by 100 m (e.g., L4-05 is 500 m from ground zero). SPE-1 is multiplied by 4, problem traces are zeroed out, and the bar in bottom right is 0.1 s. Note that the vertical component is positive-down (per geophone standards and Society of Exploration Geophysicists [SEG] convention), so first arrivals have negative polarity.

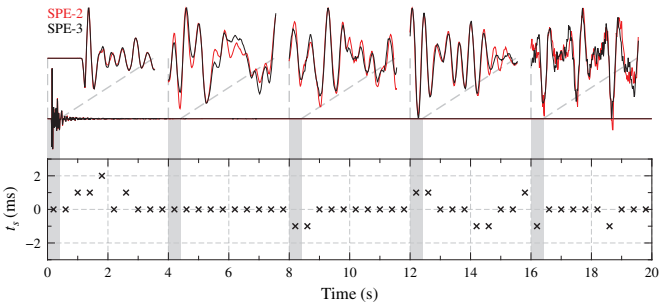

Figure 3. Recordings of SPE-2 (red) and SPE-3 (black) at station L4-05 (distance = 500 m). Blowups of the full trace show selected 0.4 s windows normalized to maximum amplitude used for the cross-correlation analysis, to determine the best shift time t_s, which is given as a function of time in the bottom panel (geophone sample interval is 2 ms).

signal, which can reduce the number of usable windows for analysis. Douma and Snieder (2006) show how to correct $R_{\max}^{(t,t_w)}$ to remove the bias due to noise. Figure 3 shows the measurement of t_s at station L4-05. The shift time measurement becomes stable, approximately, 3 s after the direct arrival, when the multiple scattering assumption is more valid.

Location perturbation from CWI

Snieder and Vrijlandt (2005) show that small changes in source location δ of explosions can be detected in a constant medium of velocity v from measurement of the correlation coefficient, since for a multiply scattered medium,

$$R_{\max}^{(t,t_w)} = 1 - \frac{1}{6}\bar{\omega}^2\frac{\delta^2}{v^2}, \tag{2}$$

in which the mean square of the angular frequency is given by

$$\bar{\omega}^2 = \frac{\int_{t-t_w}^{t+t_w}\dot{u}^2(t')dt'}{\int_{t-t_w}^{t+t_w}u^2(t')dt'}, \tag{3}$$

in which the overdot denotes time differentiation. We can test this theory with the well-recorded SPE Phase I chemical explosions, which will be presented in a later section.

Medium change from CWI

For a constant change in the velocity δv of the entire medium the mean travel-time perturbation is given by

$$\langle\tau\rangle_{(t,t_w)} = -\frac{\delta v}{v}t, \tag{4}$$

in which t is the propagation time. Equation (4) gives the relationship of shift time to velocity change for a perturbation throughout the total scattered volume from source to receiver. However, the change in velocity of the medium due to damage from a contained explosion is more localized around the source. Pacheco and Snieder (2005) derive the multiple scattering kernel K needed to predict shift time from a localized velocity perturbation as would be caused by damage. The mean travel-time perturbation at time t is then given by

$$\langle\tau(t)\rangle = \int K(\mathbf{r},t)\frac{\delta s}{s}(\mathbf{r})dV(\mathbf{r}), \tag{5}$$

in which $\delta s/s$ is the slowness perturbation at position $\mathbf{r}$ within a volume V. $K(\mathbf{r},t)$ is the multiple scattering kernel, which is dependent on a solution to the diffusion equation. Such a solution describes a pulse of energy that propagates through a medium with intensity $P(r,t)$, which in 3D can be approximated by

$$P(\mathbf{r},t) = \frac{1}{(4\pi Dt)^{3/2}}\exp\frac{-r^2}{4Dt} \tag{6}$$

(Dainty and Toksöz, 1981), in which D is the diffusion constant. The multiple scattering kernel K is then given by the normalized time convolution of P from source $\mathbf{s}$ to element $\mathbf{k}$ and from element $\mathbf{k}$ to receiver $\mathbf{r}$,

$$K(\mathbf{k},\mathbf{s},\mathbf{r},t) = P(|\mathbf{k}-\mathbf{s}|,t) * P(|\mathbf{r}-\mathbf{k}|,t), \tag{7}$$

so that, in the simple case of collocated source and receiver, K has an analytical solution given by

$$K(\mathbf{r},t) = \frac{1}{2\pi Dr}\exp\left(\frac{-r^2}{Dt}\right). \tag{8}$$

When the source and receiver are separated, K must be calculated numerically to give $\langle\tau(t)\rangle$ by equation (5). This technique is especially suited for assessing changes in velocity due to damage from the SPE Phase I explosions SPE-2 and SPE-3, where direct effects at near-regional distances are difficult to detect for these approximately one tonne shots. Results using this technique will be presented in a later section.

Source Separation of SPE-1 and SPE-2

We employ equation (2) to estimate the separation δ between SPE-1 and SPE-2. As can be seen in Figure 2, SPE-2 has a greater source–time duration than SPE-1, due to its larger yield, which effectively low-passes the recordings. In order to appropriately compare the recordings, we low-pass the SPE-1 recordings below

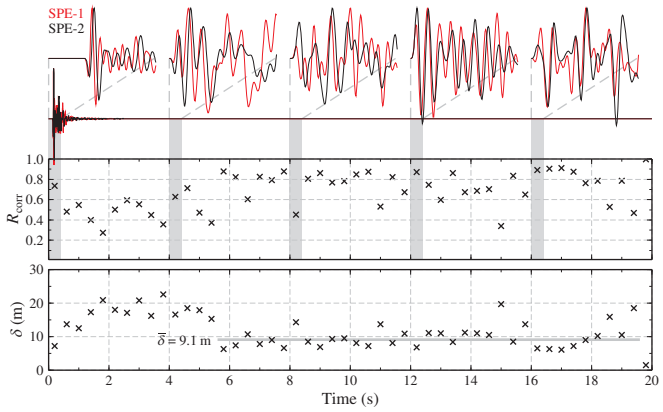

Figure 4. Recordings of SPE-1 (red) and SPE-2 (black) at station L4-05 (distance = 500 m). Blowups of the full trace show selected 0.4 s windows normalized to maximum amplitude and low-passed at 40 Hz used for the cross-correlation analysis. Middle panel is correlation corrected for noise (R_{corr}) as a function of time, and bottom panel is the calculated source displacement δ in which the average after, approximately, 6 s is 9.1 m (Actual separation is 9.4 m.).

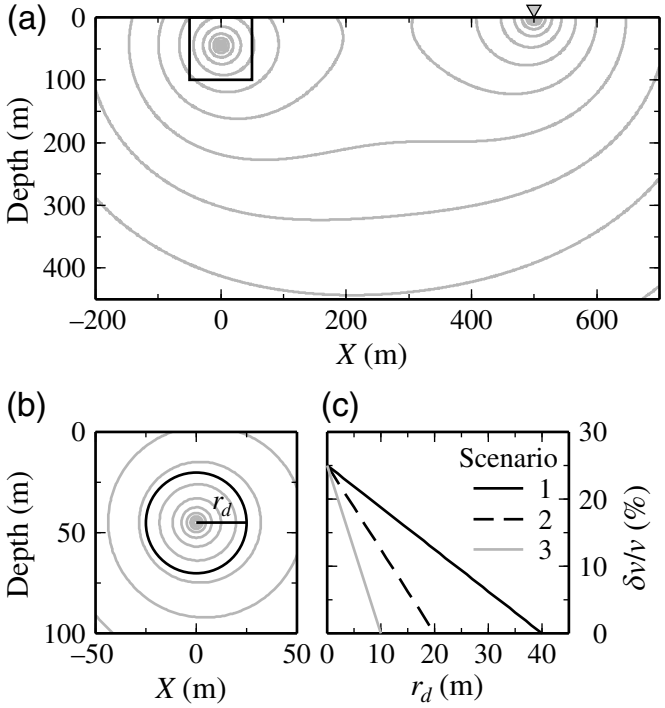

Figure 5. (a) Cross section of a multiple scattering kernel sensitivity at 10 s for a source at 45 m depth and receiver (inverted triangle) 500 m away. The box outlines the region in (b) that gives the damage region geometry used in the analysis. (c) Damage scenarios where the velocity perturbation $\delta v/v$ decreases as a function of radius r_d from the source.

the source corner frequency at 40 Hz with a six-pole causal Butterworth filter. Before measuring the cross correlation, we upsample the 500 Hz sample rate to a 1000 Hz sample rate ($\Delta t = 1$ ms). Alternatively, one could measure the shifts from the slope of the phase of the cross spectra. We find that the dominant period is about 40 ms, so we use $t_w = 200$ ms.

Figure 4 shows the source separation calculation at L4-05 for SPE-1 and SPE-2. The δ estimation becomes more stable after, approximately, 5 s, where the multiple scattering assumption is valid. The average δ after this time is 9.1 m, whereas, the actual is 9.4 m (SPE-1 centroid depth of 55.1 m – SPE-2 centroid depth of 45.7 m). The late-time estimations are less stable due to the increased effect of noise on the measurements. When we employ estimates from all the stations, the expected displacement is 9.2 m.

Medium Change due to SPE-2

In order to make a statement on medium change, we forward model possible scenarios and compare their predictions with observations. We model the perturbed region as a sphere, which is expected for such a deeply buried shot, with slowness perturbation that decreases to zero at the boundary. The diffusion constant $D = 65 \times 10^6$ m^2/s used to calculate the sensitivity kernel is from a study by Wesley (1965) at the Nevada Test Site, as reported by Dainty and Toksöz (1981). Figure 5a shows a cross section of the scattering kernel K for the SPE-2 to L4-05 source–receiver geometry where the source depth is 45.7 m and the epicentral distance is 500 m. Figure 5c shows the three localized velocity perturbation scenarios proposed as models for spherical damage. Each scenario has a slowness perturbation of 25% at the center and decreases to zero at various spherical radii. These models are then used to make predictions of $\langle \tau(t) \rangle$ at 500 m for comparison with observations at L4-05 in Figure 6. The predicted shift times for a damaged sphere where the velocity perturbation $\delta v/v$ decreases from a maximum of 25% at the center to zero at a radius of 40 m (scenario 1 in Fig. 5c) are almost an order of magnitude greater than observed. However, the predicted shift times for a damaged sphere with radius less than 10 m (scenario 3 in Fig. 5c) are less than a few record samples and are difficult to definitively observe; therefore, this scenario cannot be rejected and serves as an upper bound. Alternative scenarios that are still bounded by the observation are balanced variations of this scenario. Balanced in the sense that a stronger, smaller perturbation or a weaker, larger one will predict shift times that remain bounded by the observations. For example, a maximum perturbation of 40% with a radius of 5 m or a

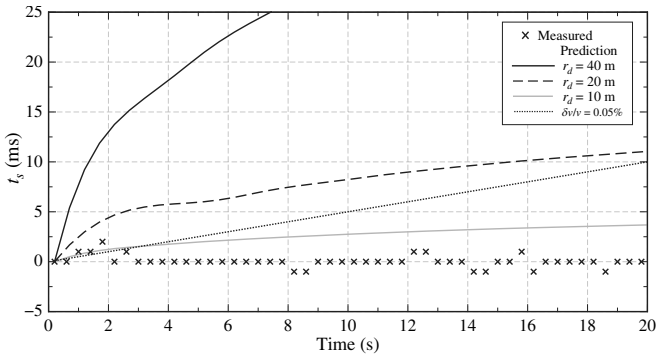

Figure 6. Shift time measurement (crosses) at L4-05 versus predictions (lines) for various localized velocity perturbation due to damage scenarios with maximum $\delta v/v = 0.25$ (see Fig. 5 for scenarios). A prediction for a whole medium (source to receiver) perturbation of $\delta v/v = 0.05\%$ from equation (4) is also given for comparison (dotted line). Scenarios with damage radius (r_d) greater than 10 m produce an observable shift time much greater than several samples (geophone sample interval is 2 ms).

maximum perturbation of 10% with a radius of 25 m are also scenarios that cannot be rejected. The feasibility of these scenarios will be discussed in the next section.

Discussion

The constraint from the CWI analysis agrees with the ground truth from geological assessment. Townsend *et al.* (2012) report damage effects out to a radius of almost 10 m, where there are distributed microfractures out to 3 m and discrete fractures from 3 to 5 m. In addition, Schwering *et al.* (2019) perform a cross-borehole change detection analysis and invert differential arrival times collected from a pair of 40 m distant boreholes for compressional velocity changes in the medium between the boreholes. The inverted image shows an approximately 25% velocity perturbation centered near the collocated SPE-2 and SPE-3 site that tapers out to zero over a 40 m wide by 20 m tall ellipsoidal region. Subsequent work by Hoots *et al.* (2020) shows that such an image could be produced by a spherical change to the medium that is not constrained by the imaging geometry. The simple spherical model presented here suggests that such a low-velocity region would be detected in the shift times of the SPE Phase I network.

Damage (or a crushed zone) around an explosion-created cavity in a high-strength material like granite extends 2–5 cavity radii around the source (Rodionov *et al.*, 1971; Office of Technology Assessment, 1989) with a radial fracture zone out to about 4–15 cavity radii (Adushkin and Spivak, 2015). Rougier and Patton (2015) show that an assumed cavity with a radius of, approximately, 1 m is consistent with the near-field observations of reduced displacement potential that are very similar for both SPE-2 and SPE-3. If we take the upper limits of damage radii, this equates to about a 5 m radius of damage (crushed zone) and a 15 m radius of radial fractures. Rougier and Patton (2015) also estimate a "bulking" region of reduced density within about 6.5 m radius that fits their model for reduced displacement potential. These scenarios are consistent with the analysis presented here. In addition, Stroujkova *et al.* (2015) found similar scaled damage radii in their study of chemical explosions in granite.

There are several reasons why the elastic scattering theory adopted here may not be applicable to the realistic deformation induced by large chemical explosions. The damage region does not behave linearly, so scatterers within this region may not contribute in accordance with the averaging theory used to derive the shift time dependence on source separation and medium change. A possible explanation for the small shift times between SPE-2 and SPE-3 is that, although, the nonlinear region changed quite a bit, the scattering medium outside this region and in the elastic regime did not change at all. However, Robinson *et al.* (2011) found success determining earthquake source separations of tens to hundreds of meters for magnitude 1–3 events from stations up to 26 km away, which certainly would have produced a nonlinear zone around the fault-slip region. And the success of applying the theory to find a fairly accurate assessment of source separation between SPE-1 and SPE-2 would argue that the theory may be applicable, such that the scattering medium is perturbed enough to prove the scattering theory valid.

Finally, the reader is referred to the outstanding work by Robinson *et al.* (2011, 2013). Not only are their aforementioned applied results relevant to this work, but their theoretical and numerical investigations of CWI also allow for determination of the criteria (scattering regime, signal to noise, and sensor bandwidth) for extending CWI to a regional context with source separations of hundreds of meters for magnitude 3–4 events from stations a few hundred meters away. Such a scenario exists for many nuclear test sites, and the use of CWI with double-difference and phase arrival techniques could improve regional location for nuclear explosion monitoring.

Conclusions

The well-controlled experimental conditions provided by the SPE allow us to test the capability of CWI to measure source medium damage and source separation. The damage caused by the, approximately, one tonne TNT-equivalent SPE-2 did not

significantly perturb the direct wave arrival time or coda waves such that a travel-time perturbation was observed using CWI. We could, however, place an upper bound on the velocity perturbation caused by any damage that is constrained to a spheroidal region smaller than 10 m radius with velocity perturbation less than 25%. This constraint is consistent with observations obtained from a drillback to the source. CWI analysis between the, approximately, 100 kg TNT-equivalent SPE-1 and, approximately, 1 tonne TNT-equivalent SPE-2 estimated the source separation between those events to be, approximately, 6–18 m, with an expected separation near 9.2 m. The actual source separation is 9.4 m. This analysis shows that CWI is a powerful technique to probe small changes in the source and medium. Future work should focus on the combined effects of damage and source separation as would be observed in a more complicated scenario.

Data and Resources

Surface seismic data from the Source Physics Experiment Phase I are provided to the Incorporated Research Institutions for Seismology (IRIS) using network identifier SN (doi: 10.7914/SN/SN). Full data and reports are also part of Assembled Datasets at IRIS (http://ds.iris.edu/SeismiQuery/assembled.phtml, last accessed May 2018 and search dataset named "Source Physics Experiment"). Some plots were made using the Generic Mapping Tools v. 4.2.2 (www.soest.hawaii.edu/gmt, last accessed September 2002). Seismic analysis was done with Seismic Analysis Code v. 7.10.5 (https://ds.iris.edu/ds/nodes/dmc/software/downloads/SAC/102-0/, last accessed October 2011).

Declaration of Competing Interests

The authors acknowledge there are no conflicts of interest recorded.

Acknowledgments

The authors are grateful for helpful comments by Associate Editor Steven J. Gibbons and two anonymous reviewers that greatly improved the article. The Source Physics Experiment (SPE) would not have been possible without the support of many people from several organizations. The authors wish to express their gratitude to the National Nuclear Security Administration, Defense Nuclear Nonproliferation Research and Development, and the SPE working group—a multiinstitutional and interdisciplinary group of scientists and engineers. The authors thank the Survey Department of Mission Support and Test Services, LLC for the ground-surface coordinates. This research was performed under the auspices of the U.S. Department of Energy by the Lawrence Livermore National Laboratory under Contract Number DE-AC52-07NA27344.

References

Adushkin, V. V., and A. A. Spivak (2015). Underground explosions, *Final Technical Report WGC-2015-03*, A. Stroujkova and P. Richards (Translators), U.S. Department of State, available at https://apps.dtic.mil/sti/pdfs/ADA627744.pdf (last accessed March 2021).

Dainty, A. M., and M. N. Toksöz (1981). Seismic codas on the earth and the moon: A comparison, *Phys. Earth Planet. In.* **26,** 250–260, doi: 10.1016/0031-9201(81)90029-7.

Douma, H., and R. Snieder (2006). Correcting for bias due to noise in coda wave interferometry, *Geophys. J. Int.* **164,** 99–108, doi: 10.1111/j.1365-246X.2005.02807.x.

Grêt, A., R. Snieder, and U. Özbay (2006). Monitoring *in situ* stress changes in a mining environment with coda wave interferometry, *Geophys. J. Int.* **167,** 504–508, doi: 10.1111/j.1365-246X.2006.03097.x.

Hoots, C. R., R. Abbott, L. Preston, H. Knox, and P. C. Schwering (2020). Near-field imaging of shallow chemical explosions in Granite using change detection methods with surface and borehole seismic data, *Technical Rep. SAND2020-4327*, Sandia National Laboratories, Albuquerque, New Mexico, doi: 10.2172/1617436.

Johnson, L. R., and C. G. Sammis (2001). Effects of rock damage on seismic waves generated by explosions, *Pure Appl. Geophys.* **158,** 1869–1908, doi: 10.1007/PL00001136.

Martin, R., P. Boyd, A. Stroujkova, M. Leidig, J. Lewkowicz, and J. Bonner (2011). Correlating near-source rock damage from single-hole explosions to seismic waves, *Proc. of the 2011 Monitoring Research Review, Ground-Based Nuclear Explosion Monitoring Technologies*, LA-UR-11-04823, available at www.osti.gov/biblio/1027453 (last accessed March 2021).

Office of Technology Assessment (1989). The containment of underground nuclear explosions, United States Congress, available at http://www.princeton.edu/~ota/disk1/1989/8909/8909.PDF (last accessed March 2021).

Pacheco, C., and R. Snieder (2005). Time-lapse travel time change of multiply scattered acoustic waves, *J. Acoust. Soc. Am.* **118,** no. 3, 1300–1310, doi: 10.1121/1.2000827.

Patton, H. J., and S. R. Taylor (2011). The apparent explosion moment: Inferences of volumetric moment due to source medium damage by underground nuclear explosions, *J. Geophys. Res.* **116,** doi: 10.1029/2010JB007937.

Poupinet, G., J.-L. Got, and F. Brenguier (2008). Monitoring temporal variations of physical properties in the crust by cross-correlating the waveforms of seismic doublets, *Adv. Geophys.* **50,** 373–399, doi: 10.1016/S0065-2687(08)00014-9.

Poupinet, G., A. Ratdomopurbo, and O. Coutant (1996). On the use of earthquake multiplets to study fractures and the temporal evolution of an active volcano, *Annali di Geofisica* **39,** 253–264, doi: 10.4401/ag-3968.

Robinson, D., M. Sambridge, and R. Snieder (2007). Constraints on coda wave interferometry estimates of source separation: The acoustic case, *Explor. Geophys.* **38,** 189–199, doi: 10.1071/EG07019.

Robinson, D. J., M. Sambridge, and R. Snieder (2011). A probabilistic approach for estimating the separation between a pair of earthquakes directly from their coda waves, *J. Geophys. Res.* **116,** no. B4, doi: 10.1029/2010JB007745.

Robinson, D. J., M. Sambridge, R. Snieder, and J. Hauser (2013). Relocating a cluster of earthquakes using a single seismic station, *Bull. Seismol. Soc. Am.* **103,** no. 6, 3057–3072, doi: 10.1785/0120130004.

Rodionov, V. N., V. V. Adushkin, V. N. Kostyuchenko, V. Nikolaevkii, A. Romashov, and V. M. Tsvetkov (1971). Mechanical effect of an underground explosion, R. Addis (Translator), United States Atomic Energy Commission, Technical Information Center, UCRL-Trans-10676.

Rougier, E., and H. J. Patton (2015). Seismic source functions from free-field ground motions recorded on SPE: Implications for source models of small, shallow explosions, *J. Geophys. Res.* **120,** 3459–3478, doi: 10.1002/2014JB011773.

Schwering, P. C., C. R. Hoots, H. Knox, R. Abbott, and L. Preston (2019). Near-field imaging of shallow chemical detonations in granite using change detection methods of borehole seismic data, *Technical Rep. SAND2019-0924*, Sandia National Laboratories, Albuquerque, New Mexico, doi: 10.2172/1493361.

Snelson, C. M., R. E. Abbott, S. T. Broome, R. J. Mellors, H. J. Patton, A. J. Sussman, M. J. Townsend, and W. R. Walter (2013). Chemical explosion experiments to improve nuclear test monitoring, *Eos Trans. A G U* **94,** no. 27, 237–239, doi: 10.1002/2013EO270002.

Snieder, R. (2004). Extracting the Green's function from the correlation of coda waves: A derivation based on stationary phase. *Phys. Rev. E* **69,** no. 4, 046610, doi: 10.1103/PhysRevE.69.046610.

Snieder, R., and M. Hagerty (2004). Monitoring change in volcanic interiors using coda wave interferometry: Application to Arenal Volcano, Costa Rica, *Geophys. Res. Lett.* **31,** doi: 10.1029/2004GL019670.

Snieder, R., and M. Vrijlandt (2005). Constraining the source separation with coda wave interferometry: Theory and application to earthquake doublets in the Hayward fault, California, *J. Geophys. Res.* **110,** B04301, doi: 10.1029/2004JB003317.

Snieder, R., A. Grêt, H. Douma, and J. Scales (2002). Coda wave interferometry for estimating nonlinear behavior in seismic velocity, *Science* **295,** 2253–2255, doi: 10.1126/science.1070015.

Stevens, J. L., and M. O'Brien (2012). Seismic wave generation and propagation from complex 3D explosion sources, *Proc. of the 2012 Monitoring Research Review, Ground-Based Nuclear Explosion Monitoring Technologies*, LA-UR-12-24325, available at www.osti.gov/biblio/1050499 (last accessed March 2021).

Stroujkova, A., J. L. Bonner, M. Leidig, P. Boyd, and R. J. Martin (2012). Shear waves from explosions in granite revisited: Lessons learned from the New England damage experiment, *Bull. Seismol. Soc. Am.* **102,** no. 5, 1913–1926, doi: 10.1785/0120110204.

Stroujkova, A., M. Leidig, and T. Rath (2015). Seismic coupling of chemical explosions in intact and fractured granite in Barre, Vermont, *Bull. Seismol. Soc. Am.* **105,** no. 1, 177–188, doi: 10.1785/0120130328.

Townsend, M. J., H. E. Huckins-Gang, L. B. Prothro, and S. N. Reed (2012). Geologic assessment of the damage zone from the seond test of the source physics experiment in Nevada, *Proc. of the 2012 Monitoring Research Review, Ground-Based Nuclear Explosion Monitoring Technologies*, LA-UR-12-24325, available at www.osti.gov/bridge/servlets/purl/1050499/1050499.pdf (last accessed March 2021).

Townsend, M. J., L. B. Prothro, and C. Obi (2011). Geology of the source physics experiment site climax stock Nevada National security site, Report prepared for *U.S. Department of Energy, DOE/NV/25946-1448*, National Nuclear Security Administration, National Center for Nuclear Security.

Wesley, J. P. (1965). Diffusion of seismic energy in the near range, *J. Geophys. Res.* **70,** 5099–5106, doi: 10.1029/JZ070i020p05099.

Manuscript received 9 February 2021
Published online 6 April 2021